ACS APPLIED MATERIALS & INTERFACES

Research Article

Cite This: ACS Appl. Mater. Interfaces 2018, 10, 29933−29942

www.acsami.org

Fast IR-Actuated Shape-Memory Polymers Using in Situ Silver Nanoparticle-Grafted Cellulose Nanocrystals

Antoniya Toncheva,*[,†,‡] Farid Khelifa,[†] Yoann Paint,[§] Michel Voué,[∥] Pierre Lambert,[⊥] Philippe Dubois,[†] and Jean-Marie Raquez*[,†]

[†]Laboratory of Polymeric and Composite Materials, University of Mons, 23 Place du Parc, Mons 7000, Belgium

[‡]Laboratory of Bioactive Polymers, Institute of Polymers, Bulgarian Academy of Sciences, 103A Academik G. Bonchev Street, Sofia 1113, Bulgaria

[§]Analysis and Characterization Unit, Materia Nova, 1 Avenue Copernic, Mons 7000, Belgium

[∥]Materials Physics and Optics, University of Mons, 20 Place du Parc, Mons 7000, Belgium

[⊥]BioElectro and Mechanical Systems Department, Free University of Brussels, 50 Avenue F.D. Roosevelt, Brussels 1050, Belgium

Supporting Information

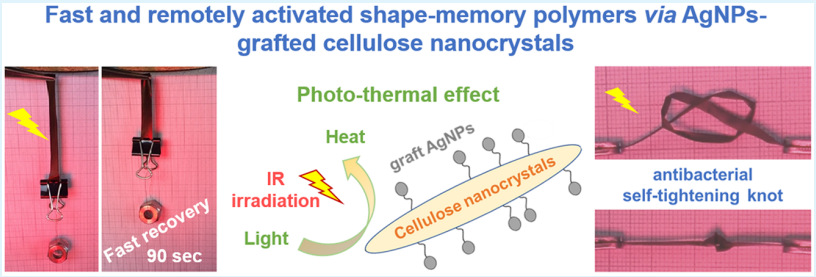

ABSTRACT: In recent years, shape-memory polymers (SMPs) have gained a key position in the realm of actuating applications from daily life products to biomedical and aeronautic devices. Most of these SMPs rely mainly on shape changes upon direct heat exposure or after stimulus conversion (e.g., magnetic field and light) to heat, but this concept remains significantly limited when both remote control and fine actuation are demanded. In the present study, we propose to design plasmonic silver nanoparticles (AgNPs) grafted onto cellulose nanocrystals (CNCs) as an efficient plasmonic system for fast and remote actuation. Such CNC-*g*-AgNPs "nanorod-like" structures thereby allowed for a long-distance and strong coupling plasmonic effect between the AgNPs along the CNC axis, thus ensuring a fast photothermal shape-recovery effect upon IR light illumination. To demonstrate the fast and remote actuation promoted by these structures, we incorporated them at low loading (1 wt %) into poly(ε-caprolactone) (PCL)-based networks with shape-memory properties. These polymer matrix networks were practically designed from biocompatible PCL oligomers end-functionalized with maleimide and furan moieties in the melt on the basis of thermoreversible Diels−Alder reactions. The as-produced materials could find application in the realm of soft robotics for remote object transportation or as smart biomaterials such as self-tightening knots with antibacterial properties related to the presence of the AgNPs.

KEYWORDS: *poly(ε-caprolactone), shape-memory polymers, IR light, cellulose nanocrystals, silver nanoparticles, plasmonic effect*

INTRODUCTION

Shape-memory polymers (SMPs) are quickly gaining their place as a new class of polymers, offering the possibility to custom-design devices with unique functionalities such as self-deployable structures, (bio)sensors, actuators, self-expanding stents, intelligent sutures, active catheters, and others.[1] Because of the presence of a permanent network, SMPs are described as being capable of memorizing a temporary shape after deformation and recovering back to their original shape upon exposure to an appropriate stimulus. Historically, the activation of the SMP was mainly related to the polymer thermal transitions, glass temperature (T_g) or melting temperature (T_m). Over the years, this concept was extended from thermal to light (UV−visible (UV−vis) and IR), electromagnetic, electrical, and other indirect heat activations, mainly via the incorporation of functional nanofillers such as plasmonic nanoparticles (NPs), magnetic nanostructures, and carbon nanotubes, respectively.[2]

Nowadays, special attention is paid to the light-triggered SMPs due to the possibility of activating them in a remote way with both high spatial and temporal resolutions using a large spectrum of light (from UV−vis to IR). In the current

Received: June 18, 2018
Accepted: August 9, 2018
Published: August 9, 2018

DOI: 10.1021/acsami.8b10159
ACS Appl. Mater. Interfaces 2018, 10, 29933−29942

literature, a plethora of original studies have been published on light-triggered SMP systems. Some of the most prominent focus on the development of polymer devices with visible and near-IR imaging modalities for soft tissue optical visualization,[3] Diels–Alder dynamic cross-linked polyurethane (PUR) structures containing polydopamine particles with conferred self-healing properties,[4] polymer systems containing photothermal fillers for improved spatiotemporal shape control under the exposure of different light illumination sequences,[5] as well as polymer composites loaded with carbon nanotubes or graphene nanoplatelets[6] for good electrical and self-driven ability. Different SMPs were described using small photoreactive molecular reversible switches such as cinnamic acid and its analogues (cinnamylidene acetic acid or *N*,*N*-bis-2-(hydroxyethyl)cinnamide or nitro-cinnamate) in PUR multiblocks[7−10] and azobenzene.[11] However, the most frequent difficulties, affecting the performances and the reproducibility in these systems, are related to the multistep synthetic approaches for active agent incorporation along the polymer backbone, the precise working wavelengths, the spatioselective geometrical position of the molecule fragments to form the cycloadditive dimers, and the required soft material properties ensuring the chain mobility. In this aspect, deserved interest was paid to the exploitation of plasmonic nanostructures derived from noble metals (silver (Ag) and gold (Au) nanoparticles (NPs), nanorods, nanowhiskers or nanowires, and others).[12,13] Characterized with large specific surface area and strong surface plasmonic resonance properties, they are readily able to absorb wavelengths in the broad spectrum range from deep UV to near IR light and to convert it into heat energy via a photothermal effect.[14,15] Depending on the interparticle distance, a new phenomenon known as "plasmon coupling" can occur, accompanied by significant change in the optical properties compared to the individual NPs.[16] Another great advantage could be their high efficiency while being used in low amounts offering the possibility to convert the light energy in a thermal one with various choices of polymer materials and manufacturing techniques.[17]

The final SMP nanocomposite properties are often related by the degree of nanofiller compatibility with the polymer matrix and the quality of their distribution and dispersion. In this aspect, noble metal NPs are the subject of a plethora of studies due to their tendency to form clusters and aggregates during the polymer processing, thus restricting the practical application of the final devices. Some of the approaches imply the surface modification of the NPs can actually affect their plasmonic properties and prevent the possibility of interacting with the adjacent nanostructures. Another problem could be the NPs detachment when incorporated in a noncovalent way within the polymer matrix (detrimental in the case of coatings). One promising approach to overcome these limitations is the combination of several nanofillers with the goal of creating new value-added structures. Cellulose nanocrystals (CNCs) were used as carrier agents for the successful nucleation and immobilization of plasmonic NPs. Naturally, they have a hydrophilic surface due to the presence of multiple hydroxyl groups that tend to stabilize metal (Ag) ions on the nanocrystal surface through complexation based on an ion–dipole interaction or passivation of the metallic surface.[18] In this way, the spontaneous NP aggregation will decrease, while reaching a higher degree of nanofiller dispersion for fast photoresponsiveness to the materials. Extracted from abundant cellulose resources, CNCs are also remarkable due to their renewability, biodegradability, low density, outstanding mechanical properties, and high surface area.[19] Another advantage to using CNCs affords the possibility to get a long-distance plasmonic effect whether plasmonic NPs are well-assembled along the CNC axis that can be achieved with existing plasmonic nanorods.[20]

Meanwhile, Ag-based plasmonic structures for the fabrication of SMP nanocomposites are still barely explored. Devices with antibacterial and enhanced mechanical properties were obtained from Ag-coordination polymer networks of isonicotinate-functionalized polyester with pyrazinamide groups.[21] Ag nanowiskers can be used in combination with a cross-linked polyacrylate layer for highly flexible transparent SMP bilayer electrodes for light-emitting diodes.[22,23] New developments in the incorporation of nanofillers are focused on the design of bi- and multilayers, resulting in flexible and fast electroresponsive PUR with shape recovery through the Joule effect.[24,25] Epoxy-based thermoset resins with improved electrothermal properties and fast electroactivated shape-recovery performance were produced by incorporating AgNPs–decorated graphene oxide assembly grafted onto carbon fibers[26] or by generating a synergistic effect of AgNPs–decorated graphene oxide structures for materials with improved electrical conductivity.[27] Other studies on the development of IR-responsive SMP composites through the incorporation of photothermal nanofillers were based on either poly(ethylene glycol)-based Au nanorods for materials with induced healable properties[28] or for self-cleaning surfaces and polarized light sensitive poly(vinyl alcohol)-based films.[29] In terms of smart material fabrication, black phosphorus in piperazine-based PUR,[30] carbon nanotubes,[31] and graphene oxide[32] were also explored for the conversion of the optical energy into heat, necessary for the shape-recovery process.

In the present work, light-responsive nanocomposites based on biocompatible poly(ε-caprolactone) (PCL_{SMP})-containing complex nanofillers such as biosourced CNCs decorated with AgNPs were designed. The permanent domains in the SMP materials laid on the networks of cross-linked PCL_{SMP} oligomers able to undergo thermoreversible Diels–Alder reactions, that is, via maleimide and furan moieties, while the switching domains result from the semicrystalline nature of the polyester. To confer high light sensitivity to the materials, CNCs were used as effective carrier agents for the NPs dispersion within the polymer matrix. Two types of complex nanofillers were designed either by simple adsorption of the AgNPs (CNC-*ad*-AgNPs) or by their grafting (CNC-*g*-AgNPs) onto the surface of the CNCs. Special attention was paid to the synthesized nanofiller optical properties as well as to their impact on the thermal, thermomechanical, and shape-memory characteristics of the resulting nanocomposite materials. The photothermal effect generated upon IR illumination (transfer of the light energy to a thermal one through the NPs plasmonic properties) made it possible to tune the material contraction or bending movement in a remote and smooth way. From an application point of view, the PCL_{SMP}/CNC-AgNPs films were studied as devices for soft robotics (for object transportation) and as biomaterials, such as a self-tightening knot for suture enclosure and antibacterial properties.

RESULTS AND DISCUSSION

It is commonly admitted that the interactions between the CNCs glucosic units and the metal NPs are relatively weak and

DOI: 10.1021/acsami.8b10159
ACS Appl. Mater. Interfaces 2018, 10, 29933−29942

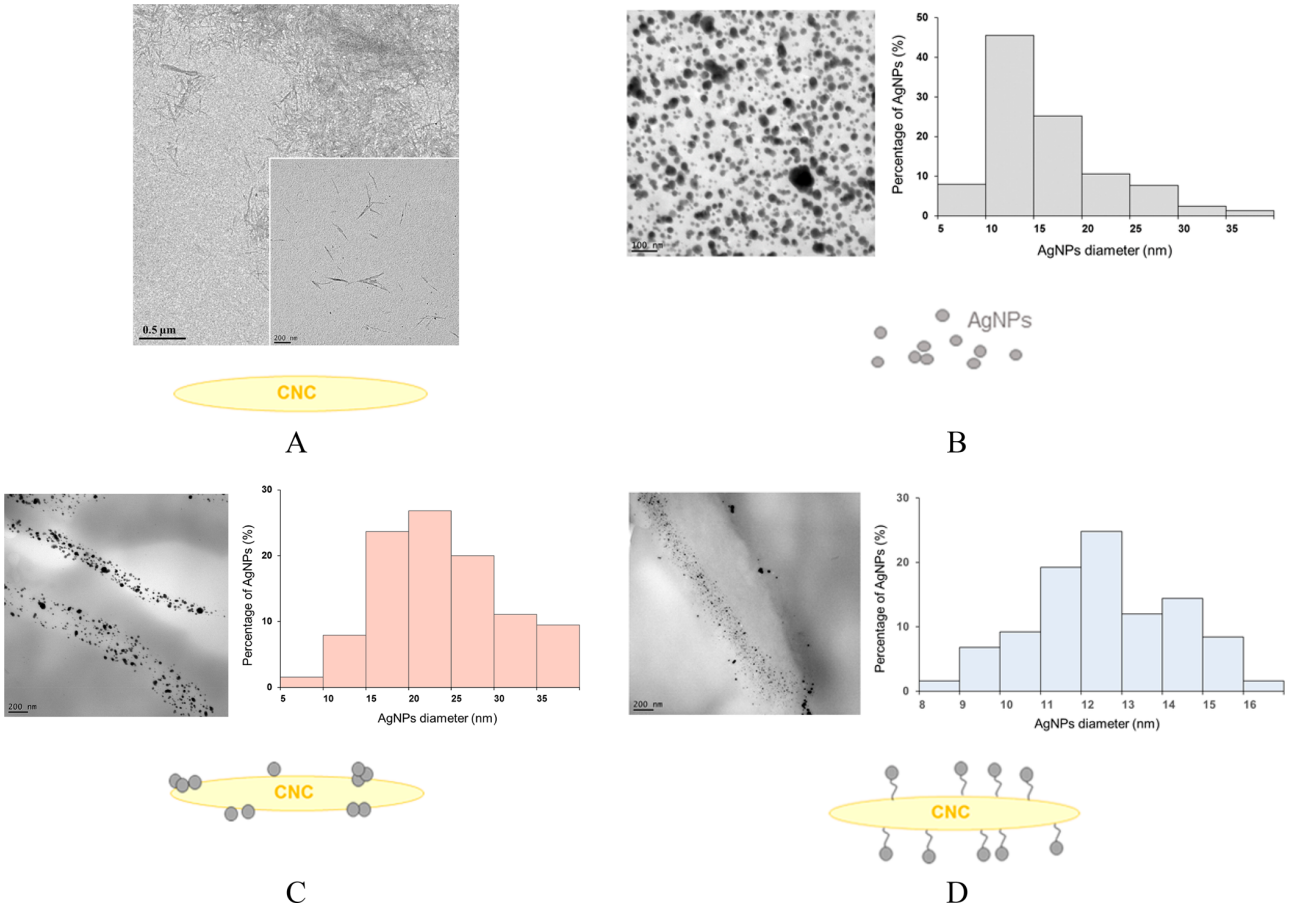

Figure 1. TEM micrographs of (A) CNCs, (B) AgNPs, (C) CNC-*ad*-AgNPs, and (D) CNC-*g*-AgNPs. Micrograph magnification: 0.5 μm and 200 nm for the inset micrograph (A) and 200 nm for (B–D). Histogram data based on at least 200 independent measurements.

reversible, which leads to a separation of the metallic/organic particles with time.[33] This reversibility could be of interest in some cases, but generally, greater efforts are paid to avoid the particle aggregation generating additional interparticle interaction by introducing surface-active nucleophile species.[34] The theory of Person et al. suggested that noble metals including Ag, characterized by a large ionic radius and a high electronegativity, can be considered as soft acids. It follows that, in the presence of soft bases, such as thiol-containing compounds (low electronegativity and small radius), the metallic particles tend to have a strong affinity and create covalent bonds. In this optic, thiol-functionalized CNCs (CNCs-SH) can be suitable candidates to stabilize efficiently the particles in a long-term time scale. In the present study, two strategies were applied for the AgNPs generation and immobilization: (i) AgNPs adsorption on the CNCs surface (CNC-*ad*-AgNPs) by direct reduction of Ag ions in the presence of $NaBH_4$ and (ii) AgNPs grafted on the CNCs surface (CNC-*g*-AgNPs) by CNCs surface modification with thiol groups and subsequent reduction of Ag ions in the presence of the reducing agent. In the first procedure, the generated nanospheres were electrostatically immobilized, and in the second, they were covalently bonded on the CNCs-SH surface (an esterification reaction between the hydroxyl group of the CNCs and 3-mercaptopriopionic acid). The morphological analyses of the modified CNCs revealed interesting structural characteristics. First, the CNCs as a reference were described with a thickness of 15 ± 3 nm and a length of 157 ± 35 nm (Figure 1A).

It was found that the applied method led to the production of AgNPs with a narrow size distribution as evidenced by the histogram presented in Figure 1B. In the case of the CNC-*ad*-AgNPs, because of the uncontrolled adsorption of the NPs, the deposition of the particles was irregular: NPs with various sizes (between 10 and 25 nm) and aggregate formation (nanostructures with a diameter above 30 nm) were observed along the surface of the packed CNCs (Figure 1C). In contrast, the stabilized structures of CNC-*g*-AgNPs tend to mimic "Ag nanorod-like" architectures with regular deposition of NPs and a uniform diameter distribution of 11–12 nm (Figure 1D and Figure S1: CNC-*g*-AgNPs width of 25 nm and length ranging from 100 to 250 nm).

As a next step and with the aim to develop fast-IR actuated nanocomposites, it was of importance to find if the nanoarchitecture differences between the modified CNCs have an impact on the polymer material optical properties. From the literature survey, it is established that isolated noble metal NPs have only one plasmonic resonance due to their symmetry, but depending on the supramolecular assembly, they can form new resonances.[35] Their plasmonic characteristics also depend on their size, shape, dielectric environment, and level of electromagnetic interaction with other particles in close proximity.[36] More complex structures with anisotropic geometry (cylinders, nanorods, nanoprisms) present two

DOI: 10.1021/acsami.8b10159
ACS Appl. Mater. Interfaces 2018, 10, 29933–29942

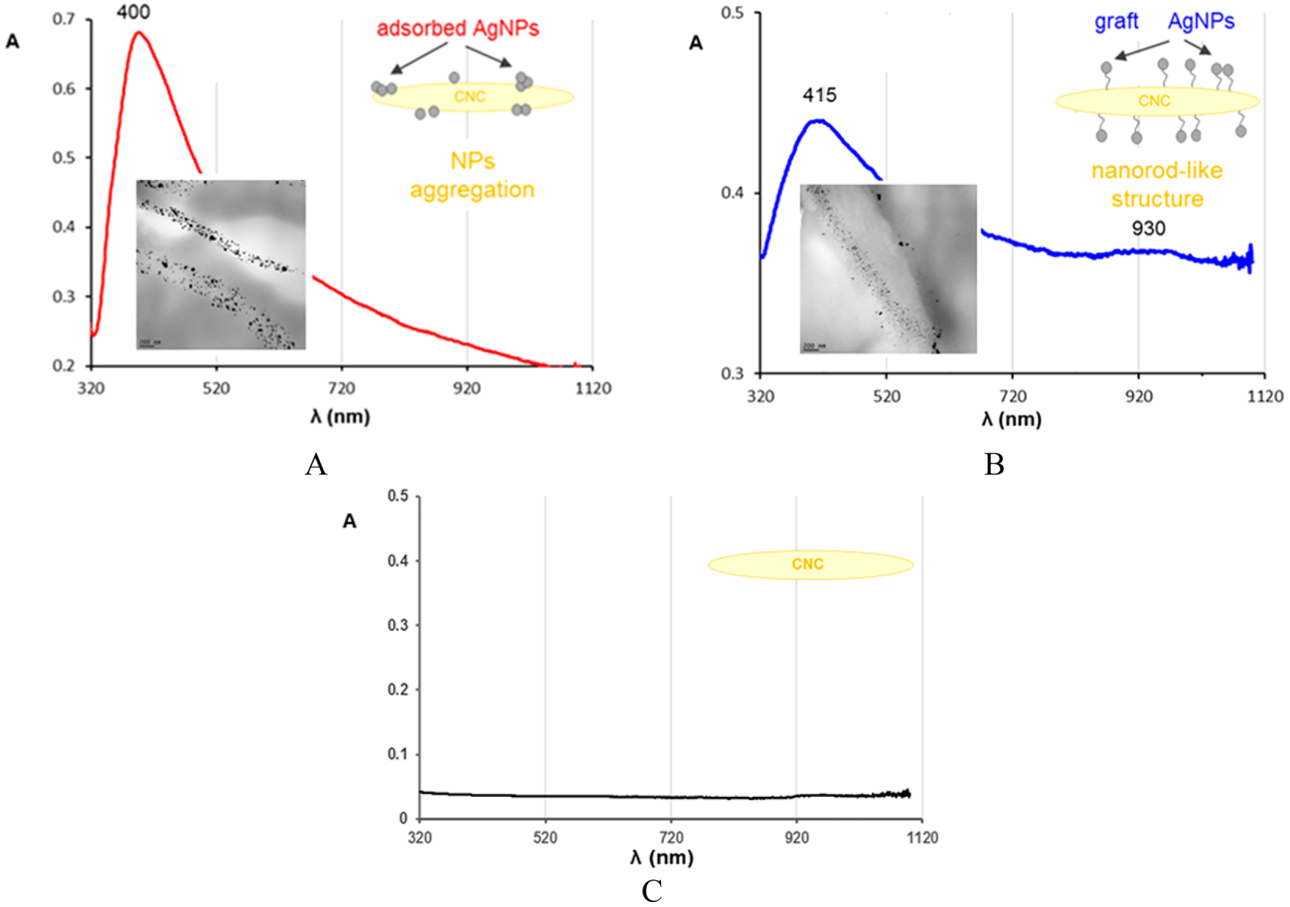

Figure 2. UV−vis and IR spectra of (A) CNC-*ad*-AgNPs, (B) CNC-*g*-AgNPs, and (C) CNCs suspensions (0.25 mg/mL) in distilled water.

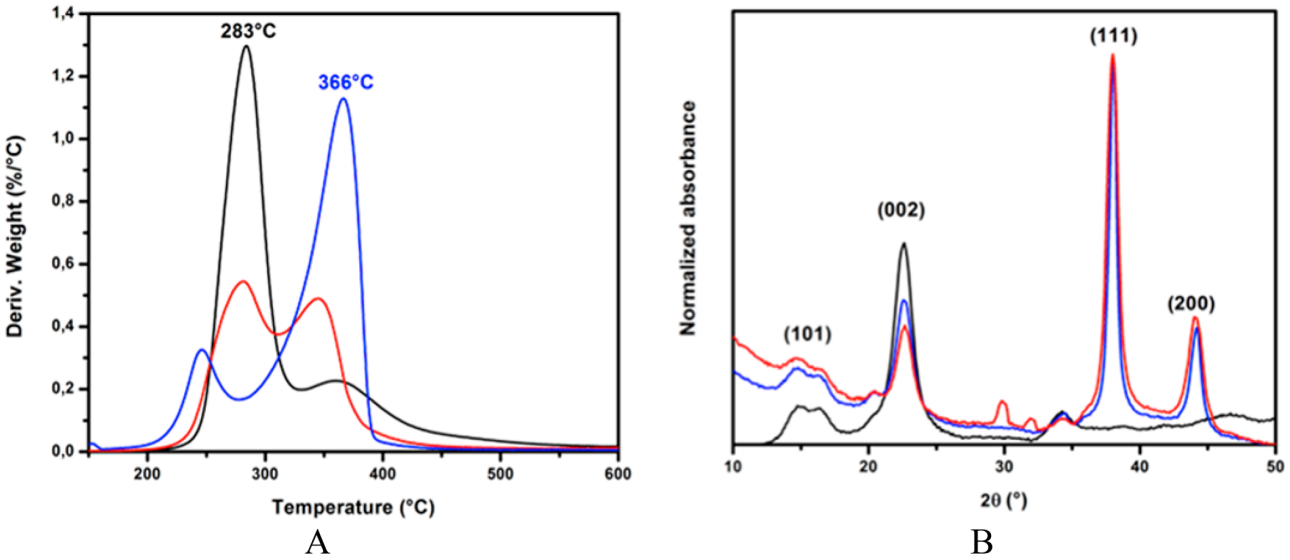

Figure 3. (A) TGA first-derivative curves performed under nitrogen and (B) XRD diffractograms of neat CNCs (black line), CNC-*ad*-AgNPs (red line), and CNC-*g*-AgNPs (blue line) samples.

plasmon absorptions: longitudinal and transverse ones situated at higher wavelengths.[37] To correlate the transmission electron microscopy (TEM) findings with the material optical features, UV−vis and IR spectrophotometry studies were performed. For the CNC-*ad*-AgNPs, a single absorption band (centered at 400 nm) was registered, as a signature of adsorbed spherical nanostructures (Figure 2A). Grafting AgNPs on the nanocrystal surface resulted in a red shift of the band, plasmon

DOI: 10.1021/acsami.8b10159
ACS Appl. Mater. Interfaces 2018, 10, 29933−29942

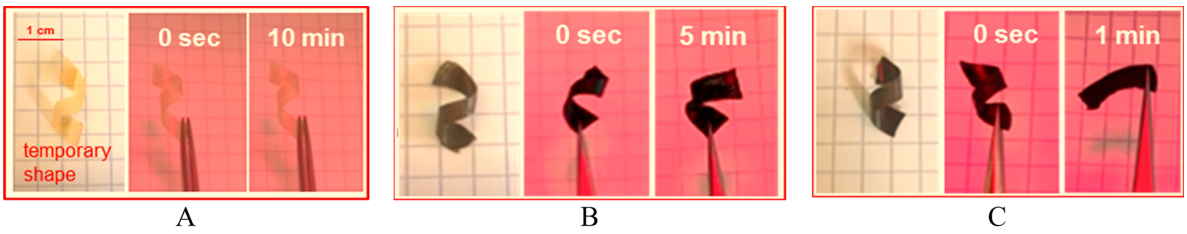

Figure 4. Digital images of the nanocomposite films corresponding to their spiral-like temporary shape and the shape-recovery process upon IR illumination: (A) PCL_{SMP} film, (B) PCL_{SMP}/CNC-*ad*-AgNPs film, and (C) PCL_{SMP}/CNC-*g*-AgNP film.

excitation along the nanofiller longer axis (415 nm) and the appearance of a second absorption broad band with low intensity at 930 nm (Figure 2B). This spectral footprint was additional evidence for the presence of a "nanorod-like" structure, where the adjacent NPs (along the nanocrystal surface) were situated at a distance sufficient enough to interact and generate a coupling plasmonic effect. Within these features, we demonstrated that it was possible to increase the nanofiller absorption window by simply modifying the type of NPs immobilization on the nanocrystal surface. Suspension of CNCs did not present an absorption maximum (Figure 2C). Having this in mind, the idea to produce a SMP with fast light responsiveness and good shape recovery was subsequently investigated.

The complex nanofillers were further characterized by Fourier transform (FT)-IR spectroscopy, and the spectra of the CNCs before and after their modification with 3-mercaptopropionic acid are presented in Figure S2. In the case of the neat nanocrystals, the characteristic band for OH stretching was noticed at 3400 cm^{-1}, and the one for C−O stretching was found between 900 and 1100 cm^{-1}. Thiol-modified CNCs presented the same characteristic bands, as well as a stretching band for the ester carbonyl group (1730 cm^{-1}). Energy-dispersive X-ray spectroscopy (EDX) analyses performed on the functionalized CNCs showed an atomic percentage of 0.8% sulfur (1.7 wt %), confirming that approximately one hydroxyl group per three anhydrous glucose units was the subject of chemical modification. In addition, C_{1s} X-ray photoelectron spectroscopy (XPS) analyses confirmed that the ester (−COO−) bond contribution increases after SH functionalization of CNCs through an esterification reaction (Figure S3 and Table S1). Evidence for the covalent bonding of AgNPs on the surface of the CNCs-SH was obtained from the S_{2p} XPS spectra: the characteristic maximum for the S−metal bond was registered at 162.5 eV (free SH groups were observed at 163.6 eV in the case of CNCs-SH; Figure S4). The presence of sulfate in the CNC samples was registered at 169.2 eV, and a less intensive peak for sulfide was measured at 164.5 eV. CNC-*ad*-AgNPs presented XPS spectra maxima at the same binding energy as in the case of the CNCs. These results were in agreement with the existing scientific literature.[38,39] The thermogravimetric analysis (TGA) thermograms under nitrogen atmosphere were performed for CNCs, CNC-*ad*-AgNPs, and CNC-*g*-AgNPs (Figure 3; raw data presented in Figure S5). Two degradation temperatures were mainly observed between 200 and 300 °C, related to the depolymerization, dehydration, and decomposition of the glycosyl units bearing the sulfate groups. On the basis of the EDX analyses, it was estimated that the values of the Ag wt % in the CNC-*ad*-Ag and CNC-*g*-AgNPs were 20 and 26 wt %, respectively. Information about the crystalline structure of the nanofillers was extracted from X-ray diffraction (XRD) diffractograms, where 2θ angles were varied from 10° to 50° (Figure 3). The specific patterns indicate highly crystalline structures with three characteristic peaks for CNCs at 2θ of 22.9° (002), 15.0° (101), and 16.7° (101). By applying the amorphous subtraction method, it was possible to calculate the degree of crystallinity, which decreased slightly for the decorated CNCs (87% for neat CNCs vs 75% for both modified CNCs). The presence of Ag was evidenced by the presence of a high intensive diffraction peak at 38.0° affirming the formation of the cubic crystal system (111) and a peak at 44.1° corresponding to the (200) plane.

In this study, the PCL_{SMP} nanocomposite was obtained by the solvent-casting technique, and both CNC-*ad*-AgNPs and CNC-*g*-AgNPs were added in a way that the total amount of AgNPs represented 1 wt % of the polymer matrix. Because the CNCs are known for their mechanical reinforcement effect when incorporated into polymer materials,[40] we investigated their impact on the films thermomechanical properties by performing dynamic mechanical thermal analysis (DMTA). The values of the storage modulus (E') for both nanocrystals containing materials were higher compared to the PCL_{SMP} film for temperatures above room temperature (Figure S6 and Table S2). Two plateau transitions were observed: one characteristic transition for the rubberlike plateau (from −40 to 30 °C) and a second one revealing the formation of the network with increased values of tan δ (above the T_m of 50 °C). In addition to this, it was found that the presence of the nanofillers does not affect significantly the material thermal properties and leads to a slight decrease in the degree of crystallinity, from 45% for the PCL_{SMP} film to 37% and 39% for PCL_{SMP}/CNC-*ad*-AgNPs and PCL_{SMP}/CNC-*g*-AgNPs, respectively (Figure S7 and Table S3).

Afterward, the light responsiveness of the composite films was studied after fixing the film in a spiral-like temporary shape. The noninvasive IR illumination (simple IR lamp) was in the range from 780 to 1400 nm with a source power of 150 W. To ensure that the shape recovery of the samples resulted only from the conversion of the light energy into heat, the distance between the source and the samples (35 cm) was chosen in a way that the temperature at the sample surface did not exceeded more than 37 °C (T_m of the PCL_{SMP} systems at around 50 °C). The PCL_{SMP} as a reference did not present any actuation event despite a light exposure of 10 min (Figure 4A). For the PCL_{SMP}/CNC-*ad*-AgNPs nanocomposite, a certain shape-memory effect is obtained, but the recovery process remained incomplete even after 5 min of illumination (Figure 4B), and for the PCL_{SMP}/CNC-*g*-AgNPs film, a fast and full-size recovery was reached in less than 1 min (Figure 4C). The obtained data revealed a greater heating efficiency for remote activation under IR-light illumination for the nanocomposites

DOI: 10.1021/acsami.8b10159
ACS Appl. Mater. Interfaces 2018, 10, 29933−29942

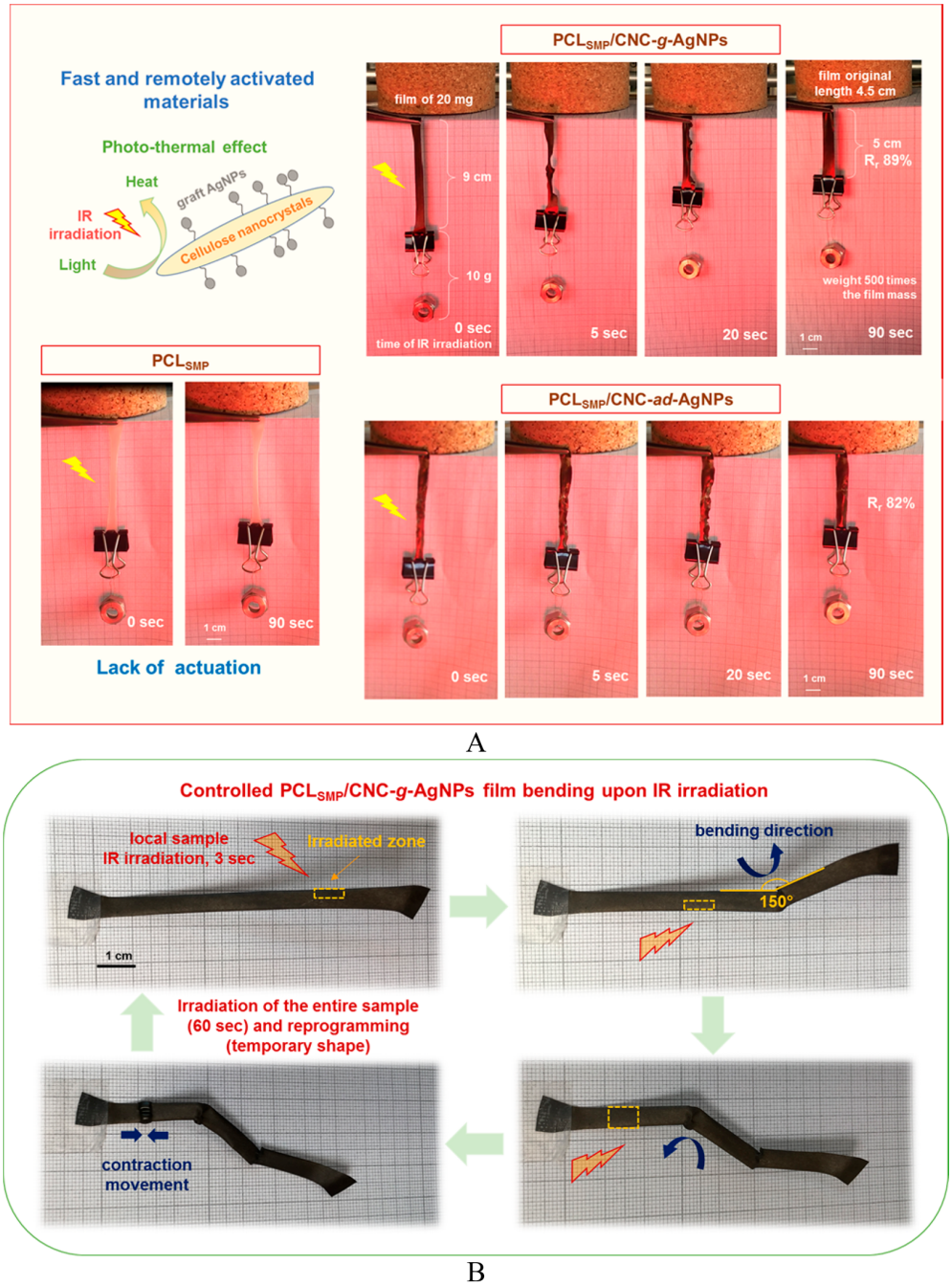

Figure 5. (A) Digital images of PCLSMP-based films actuated upon IR illumination for remote object transportation and (B) spacial control of the bending direction upon local activation.

containing the grafted AgNPs. An interpretation for the faster shape recovery of PCL_{SMP}/CNC-*g*-AgNPs was the occurring coupling plasmonic effect within the adjacent AgNPs. Therefore, the light-to-heat energy conversion allowed the materials to reach their initial shape by melting the crystalline phase within the polymer network, which in turn released the stress stored within the temporary shapes of the films. The lower degree of the PCL_{SMP}/CNC-*ad*-AgNPs actuation could be explained with the lower specific surface area of the adsorbed NPs (scattered size distribution and a tendency for the formation of aggregates) resulting in lower thermal conductivity. This light-to-heat conversion phenomena has been described by Lu et al.[41] More information about the film one-way shape-memory DMTA spectra can be found in Figure S8 and Table S4.

Regarding the material application, we performed further tests for object transportation (Figure 5A). For this purpose, the film made of PCL_{SMP}/CNC-*g*-AgNPs was stretched (strain of 100%), and the temporary shape was fixed upon cooling. The IR-light activation of the system was fast and contactless. Combined with the good mechanical properties of the materials, it was possible to develop forces sufficient enough

DOI: 10.1021/acsami.8b10159
ACS Appl. Mater. Interfaces 2018, 10, 29933−29942

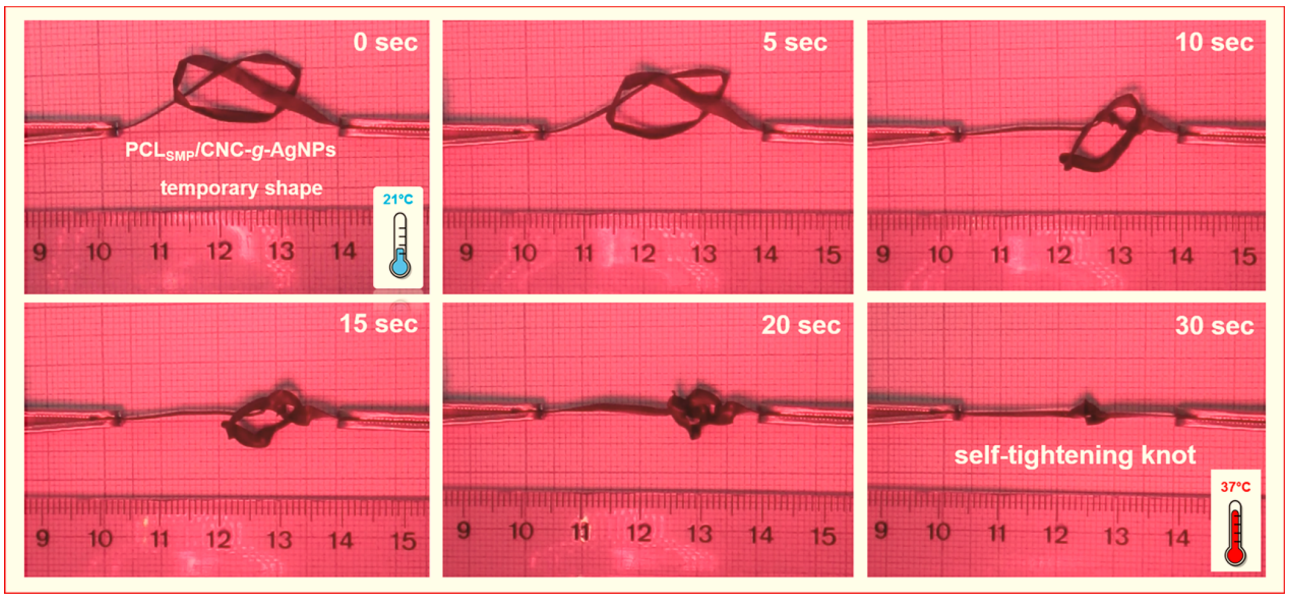

Figure 6. Self-tightening properties of the CNC-*g*-AgNPs-loaded PCL$_{SMP}$ materials upon IR illumination.

to execute mechanical work by lifting up a weight 500 times higher than the film mass for less than 90 s. This procedure was reversible and reproducible upon several stimuli exposure cycles with a good R_r value of ∼90%. The mechanical properties of the described PCL$_{SMP}$ system were comparable to other light-activated materials such as the thermosensitive SMP of cross-linked branched oligo(ε-caprolactone) loaded with AuNPs (up to 1 wt %) and lifting 350 times its weight[42] or to laser-activated cross-linked poly(ethylene oxide) containing 0.5 wt % AuNPs elevating a weight of 5 g and a bending angle of 30°.[43] As expected, the reference film of PCL$_{SMP}$ did not present an actuation, and the observed efficiency of the PCL$_{SMP}$/CNC-*ad*-AgNPs one was lower (R_r = 82%). Even more interesting was the possibility of generating controlled bending or contraction of the films upon local surface illumination by using of a mask and a standard IR-light source (Figure 5B). This multistep shape recovery demonstrates the film sensors behavior for specific light detection, where short time exposure (e.g., 3 s) can be related to a given bending angle (150°) or contraction movement. The complex geometrical shaping was explained with the temperature gradient created upon the local illumination (light-to-heat transformation through the NPs plasmonic properties), generating light-controlled release of the stored strain energy and anisotropic polymer chain relaxation.[43] In this way, the potential applications of the PCL$_{SMP}$ systems as remotely controlled complex structures such as actuators for the soft-robotic field or for the fabrication of three-dimensional-printed objects applying the fused deposition method were outlined. Another advantage of this study is the use of a commercially available light source without aiming any precise wavelength or intensity of the illumination (as in the case of lasers).

To go further in to the material application, we investigated their possible use as biomaterials with self-tightening and antibacterial properties. Promising elements in this direction were the biocompatible nature and medical use of PCL and AgNPs and the excellent tissue penetration ability of the noninvasive near-IR light.[44] For this purpose, samples of PCL$_{SMP}$ filled with CNC-*g*-AgNPs with a rectangle shape were heated at a temperature close to the polymer T_m, stretched at 100% of the deformation, and fixed in a knotlike-shaped structure upon cooling (Figure 6A). Both extremities were fixed immobile, and IR illumination was applied for fast shape recovery accompanied by self-tightening suture behavior for wound enclosure, while the light source thermal heating did not exceed 37 °C. This simple noninvasive one-step procedure presented an advantage compared to the previously reported data on self-tightening the thermoplastic SMP fiber, where gradual increasing of the temperature (from 20 to 40 °C) was needed.[45] Known for their antibacterial effect, AgNPs are one of the most promising antimicrobial agents.[46] Here, we determined the nanofiller minimal inhibitory concentration (MIC) to be 16 μg/mL against Gram-positive bacteria such as *Bacillus subtilis*. The antibacterial effect was evidenced by the appearance of a zone of inhibition (20.3 ± 0.3 mm) around the cellulose disks (Figure S9). As positive controls, different antibiotics were used (tylosin: 20.3 mm; sulfamidine: 18.2 mm; oxytetracycline: 21.5 mm; and streptomycin: 16.3 mm).

CONCLUSION

In this work, fast-actuated and photosensitive PCL shape-memory materials loaded with AgNPs-decorated CNCs were designed. The polymer matrix permanent domain was based on functionalized polyester oligomers able to undergo thermoreversible Diels−Alder reactions. The complex nanofillers were obtained after applying two types of architectural approaches: (i) adsorption of the AgNPs on the CNC surface or (ii) controlled grafting of the AgNPs on thiol-functionalized CNCs. The CNC-*g*-AgNPs "nanorod-like" morphological characteristics allowed the generation of a plasmonic coupling effect between the individual NPs resulting in relevant optical properties for this nanofiller. The incorporation of the nanofillers enhanced the material thermomechanical properties, as well as their light responsiveness, while keeping unchanged the polymer network thermal transitions (T_g and T_m). In terms of applications, the PCL$_{SMP}$-based systems were studied as actuators in the field of soft robotics for object

DOI: 10.1021/acsami.8b10159
ACS Appl. Mater. Interfaces 2018, 10, 29933−29942

catching and transportation and as biomaterials such as antibacterial self-tightening knots.

METHODS

Materials. For the production of the films, α,ω-dihydroxyl poly(ε-caprolactone) (PCL-diol; CAPA2402, M_n = 4000 g mol^{-1}) and $\alpha,\alpha',\omega,\omega'$-tetrahydroxyl poly($\varepsilon$-caprolactone) (PCL-tetraol; CAPA4801, M_n = 8000 g mol^{-1}) were used. The PCL oligomer chain end-functionalization was realized using 1-(3-hydroxylpropyl)-1*H*-pyrrole-2,5-dione (MAL(OH), prepared from 3-aminopropan-1-ol (Acros), exo-3,6-epoxy-1,2,3,6-tetrahydrophtalic anhydride (Sigma-Aldrich), and ethanol 96% vol (VWR)) and furfuryl isocyanate (Sigma-Aldrich). Dimethylformamide (DMF, Sigma-Aldrich, 99.8%), sulfuric acid (H_2SO_4, VWR, 65%), $NaBH_4$ (VWR), and $AgNO_3$ (Merck) were used as received. Pure ramie fibers were obtained from Stucken Melchers GmbH & Co.

Preparation of CNCs and CNCs-SH. For this study, 60 g of purified ramie fibers were cut into small pieces and treated with 1000 mL of a 4% NaOH solution at 80 °C for 2 h to remove any residual contaminants. The fibers were then submitted to acid hydrolysis with 800 mL of sulfuric acid solution (65%) at 55 °C for 30 min under continuous mechanical stirring. The obtained suspension was filtered off through a sintered glass no. 1 to remove any macroscopic fragments from the unhydrolyzed fibers. The suspension was thoroughly washed with water by centrifugation and dialyzed against deionized water until neutrality. The suspension was concentrated to 4 wt %, and this constituted the stock suspension. Thiol-modified CNCs were prepared by mixing 10.16 g of 3-mercaptopropanoic acid with 8 mL of acetic anhydride, 1.92 mL of glacial acetic acid, and 0.04 mL of concentrated sulfuric acid in a round-bottom flask (50 mL) cooled to room temperature. Next, 0.5 g of dried CNCs was added to the mixture under stirring, and the temperature of the reaction was increased to 40 °C. After 3 days of reaction, the precipitated thiol-modified CNCs (mercaptopropanoyl CNCs or CNCs-SH) were washed with methanol and then with distilled water through several centrifugation cycles (10 min at 10 °C and 10 000 rpm). Again, the suspension was concentrated to 4 wt % as stock suspensions. The size of the CNCs was measured from the TEM micrographs via ImageJ software.

Synthesis of CNC-*ad*-AgNPs and CNC-*g*-AgNPs. The previously obtained CNCs or CNCs-SH aqueous suspensions were subject to several solvent-exchange procedures from water to DMF: 5 g of DMF was added to 5 g of the aqueous suspension of the CNCs or CNCs-SH. After this step, the mixture was transferred to a 100 mL flask, and the water was evaporated using a rotavapor. The obtained suspensions were ultrasonicated for 5 min in order to redisperse both the CNCs and CNCs-SH. Afterward, for 1 g of the CNCs or CNCs-SH, 30 mL of $AgNO_3$ solution (10^{-2} mol L^{-1}) was added under stirring for 1 h. Then, 3 mL of $NaBH_4$ solution (10^{-2} mol L^{-1}) was poured in, and the solution was mixed for 1 h. The produced CNC-*ad*-AgNPs and CNC-*g*-AgNPs nanofillers were washed with distilled water through several centrifugation cycles (10 min at 10 °C and 10 000 rpm), and as a final step, the nanofillers were subjected to a freeze-drying procedure. The size of the adsorbed or the grafted AgNPs (at least 200 individual NPs) was measured from the TEM micrographs using ImageJ software.

Synthesis of Chain End-Functionalized PCL. The synthesis of the chain end-functionalized PCL and the production of the thermoreversible PCL-based networks were performed according to a previously reported procedure.[47] In brief, PCL-tetraol oligomers were end-functionalized with furfuryl moieties (PCL(FUR)$_4$) in bulk overnight in the presence of an excess of furfuryl isocyanate (1.5 equiv) at 110 °C in a 250 mL preconditioned flask under an inert atmosphere. Afterward, the oligomers were dissolved in CH_2Cl_2 and poured in to an excess of cold methanol in order to remove the excess of the nonreacted furfuryl isocyanate. For the synthesis of maleimide-functionalized PCL (PCL(MAL)$_2$), PCL-diol, 1-(3-hydroxylpropyl)-1*H*-pyrrole-2,5-dione, and methylene diphenyl diisocyanate were introduced into a 15 cm^3 twin-screw DSM microcompounder at 55 °C with a twin-screw rotation speed of 30 rpm under nitrogen flow. The reaction was completed in 40 min with a constant temperature of 140 °C and a rotation speed of 70 rpm. The residual protected maleimide chain ends were deprotected, and furan was removed by placing the polymer matrix in an oven under vacuum at 110 °C overnight.

Processing of CNC-AgNPs-Containing Films. Films were processed using the casting/evaporation method involving DMF as the solvent. A 1 g amount of the PCL-based matrix (0.62 g of PCL(Mal)$_2$ and 0.38 g of PCL(Fur)$_4$) was dissolved in 10 mL of DMF, and then, the desired amounts of CNC-*ad*-AgNPs (43.3 mg) or CNC-*g*-AgNPs (81.5 mg) were added to achieve AgNPs of 1 wt % with respect to the total material weight. Then, the solutions were poured into Teflon plates before being casted in an air-circulating oven at 60 °C overnight. Finally, the films with thicknesses of 0.8 mm were prepared by compression molding (manual Carver hydraulic press) using circular molds with a diameter of 100 mm and a thickness of 0.8 mm. After a compressing step (80 °C for 5 min), the films were kept for 3 min at 10 bar and under 1 bar during the overnight cooling step (progressive cooling to ambient temperature to reform Diels–Alder cross links).

Characterizations of the Nanofillers and the Nanocomposite Films. Morphological studies of the synthesized nanofillers and the obtained SMP nanocomposites were performed by TEM (Philips CM200) with an acceleration voltage of 20 kV. The UV–vis and the IR spectra of the nanofiller aqueous suspensions (CNCs, CNC-*ad*-AgNPs, and CNC-*g*-AgNPs; 0.25 mg/mL concentration) were obtained on a Thermo Genesys 10S apparatus in the range from 300 to 1100 nm. FT-IR spectra were recorded on a ATR-mode Bruker Tensor 17 spectrometer from 4000 to 600 cm^{-1} with a resolution of 4 cm^{-1} and an accumulation of 32 scans. TGA measurements were taken on a TGA Q5000 apparatus (TA Instruments) with an ~10 mg sample heated from room temperature up to 800 °C at 10 °C min^{-1} under a nitrogen or oxygen flow. Differential scanning calorimetry (DSC) measurements were performed under nitrogen flow by using a DSC Q2000 differential scanning calorimeter (TA Instruments). The thermal characteristics of the films were studied from −80 to 200 °C at a heating rate of 10 °C min^{-1}. XPS measurements were performed on a Versaprobe PHI 5000 hemispherical analyzer from Physical Electronics with a base pressure of 10^{-7} torr. During the analysis, the XPS spectra were collected at an angle of 45° with respect to the electron energy analyzer mode (23.50 eV). All the spectra were recorded using monochromatic Al Kα radiation (beam size of 100 mm and energy resolution of 0.6 eV), while calibrating the binding energy scale with respect to the C_{1s} peak (285 eV) of the samples. To avoid the sample surface charging, a built-in electron gun and an argon ion neutralizer were used. XRD analyses were performed on a powder diffractometer Siemens D 5000 using Cu Kα radiation at room temperature in the range of 2θ = 10–50° at a scanning rate of 2° min^{-1}.

The light responsiveness of the materials was studied after programming rectangle samples (15 × 5 × 0.8 mm^3) in a spiral-like temporary shape and illuminating them with an IR-lamp source (Lamp Petra IR 11, 780–1400 nm; 150 W). During this procedure, the distance between the samples and the light source was kept of 35 cm corresponding to 37 °C of heat illumination. The thermomechanical properties of the films were determined using a Q800 DMTA apparatus (TA Instrument) in multistrain mode in order to evaluate the storage and loss modulus as well as the tan δ. Each specimen was cut in a rectangular shape (30 × 5 × 0.8 mm^3) and analyzed under ambient atmosphere in the temperature range from −80 to 65 °C.

The object transportation tests were performed using a rectangle-shaped films (40 × 10 × 0.8 mm^3; 20 mg) and stretching it to 100% of the strain deformation. Afterward, a weight of 10 g was attached to the film in its temporary shape, and IR illumination was applied. The fixity and recovery ratio were calculated using Equations S2 and S3 (Supporting Information). By using a specially designed mask, it was possible to locally illuminate the sample and generate controlled bending or contraction movement. The bend angle and the length of the sample at different shape-recovery steps were calculated using the

DOI: 10.1021/acsami.8b10159
ACS Appl. Mater. Interfaces 2018, 10, 29933–29942

software program ImageJ. In the case of the self-tightening knot test, the sample was stretched at 100% of the strain deformation and put in a knotlike shape, both of the sample extremities were fixed immobile, and then, IR illumination was applied.

The antimicrobial activity of the nanofillers (32.5 μg/mL) and their MIC was tested at different dilutions against the pathogenic Gram-positive microorganism *B. subtilis*. The zones of inhibition were determined by in vitro studies using a standard solid medium (DIFCO Laboratories). Then, the surface of the solid agar was inoculated with the bacterial suspension (target concentration of 1×10^7 spores mL^{-1}), and discs with a diameter of 10 mm were deposited carrying the nanofillers or the positive control of antibiotics (tylosin, sulfamidine, oxytetracycline, and streptomycin). The Petri dishes were incubated for 24 h at 37 °C, and the average diameters of the zones of inhibition around the discs were measured using the software program ImageJ.

■ ASSOCIATED CONTENT

Supporting Information

The Supporting Information is available free of charge on the ACS Publications website at DOI: 10.1021/acsami.8b10159.

TEM micrographs; FT-IR spectra; XPS data; TGA thermograms; DMTA data (themomechanical properties and shape-memory effect); DSC data; and microbiological tests (PDF)

■ AUTHOR INFORMATION

Corresponding Authors

*E-mail: antoniya.toncheva@umons.ac.be.
*E-mail: jean-marie.raquez@umons.ac.be.

ORCID

Antoniya Toncheva: 0000-0001-5466-2817
Jean-Marie Raquez: 0000-0003-1940-7129

Notes

The authors declare no competing financial interest.

■ ACKNOWLEDGMENTS

J.-M. R. as a F.R.S.-FNRS research associate and the LPCM thank the Belgian Federal Government Office of Science Policy (SSTC-PAI 6/27) for general support and are much indebted to both Wallonia and the European Commission "FSE and FEDER" for financial support in the frame of Phasingout Hainaut. A. T. thanks the BEWARE (BElgium WAllonia REsearch, project convention no. 410161) Fellowships Academia programme cofunded by the COFUND programme of the European Union (FP7-Marie Curie Actions) for financial support. The authors are grateful to the "Région Wallonne" in the frame of the VALICELL, FEDER-SINOPLISS, and FEDER-POLYTISS projects for financial support.

■ REFERENCES

(1) Wang, W.; Liu, Y.; Leng, J. Recent Developments In Shape Memory Polymer Nanocomposites: Actuation Methods And Mechanisms. *Coord. Chem. Rev.* **2016**, *320*−*321*, 38−52.

(2) Manouras, T.; Vamvakaki, M. Field Responsive Materials: Photo-, Electro-, Magnetic- And Ultrasound-Sensitive Polymers. *Polym. Chem.* **2017**, *8*, 74−96.

(3) Weems, A. C.; Raymond, J. E.; Easley, A. D.; Wierzbicki, M. A.; Gustafson, T.; Monroe, M. B. B.; Maitland, D. J. Shape Memory Polymers With Visible And Near-Infrared Imaging Modalities: Synthesis, Characterization And In Vitro Analysis. *RSC Adv.* **2017**, *7*, 19742−19753.

(4) Yang, L.; Lu, X.; Wang, Z.; Xia, H. Diels−Alder Dynamic Crosslinked Polyurethane/Polydopamine Composites With Nir Triggered Self-Healing Function. *Polym. Chem.* **2018**, *9*, 2166−2172.

(5) Fang, T.; Cao, L.; Chen, S.; Fang, J.; Zhou, J.; Fang, L.; Lu, C.; Xu, Z. Preparation And Assembly Of Five Photoresponsive Polymers To Achieve Complex Light-Induced Shape Deformations. *Mater. Des.* **2018**, *144*, 129−139.

(6) Zhang, Z.-x.; Dou, J.-x.; He, J.-h.; Xiao, C.-x.; Shen, L.-y.; Yang, J.-h.; Wang, Y.; Zhou, Z.-w. Electrically/Infrared Actuated Shape Memory Composites Based On A Bio-Based Polyester Blend And Graphene Nanoplatelets And Their Excellent Self-Driven Ability. *J. Mater. Chem. C* **2017**, *5*, 4145−4158.

(7) Sodhi, J. S.; Rao, I. J. Modeling The Mechanics Of Light Activated Shape Memory Polymers. *Int. J. Eng. Sci.* **2010**, *48*, 1576−1589.

(8) Habault, D.; Zhang, H.; Zhao, Y. Light-Triggered Self-Healing And Shape-Memory Polymers. *Chem. Soc. Rev.* **2013**, *42*, 7244−7256.

(9) Jin, C.; Sun, X.; Wu, L. Synthesis and Characterization of N, N-Bis (2-hydroxyethyl) Cinnamamide as a Photo-Responsive Monomer. *Des. Monomers Polym.* **2011**, *14*, 47−55.

(10) Jin, B.; Song, H.; Jiang, R.; Song, J.; Zhao, Q.; Xie, T. Programming A Crystalline Shape Memory Polymer Network With Thermo- And Photo-Reversible Bonds Toward A Single-Component Soft Robot. *Sci. Adv.* **2018**, *4*, eaao3865.

(11) Nicoletta, F. P.; Cupelli, D.; Formoso, P.; De Filpo, G.; Colella, V.; Gugliuzza, A. Light Responsive Polymer Membranes: A Review. *Membranes* **2012**, *2*, 134−197.

(12) Mishra, S. R.; Tracy, J. B. Sequential Actuation of Shape-Memory Polymers through Wavelength-Selective Photothermal Heating of Gold Nanospheres and Nanorods. *ACS Appl. Nano Mater.* **2018**, *1*, 3063−3067.

(13) Pilate, F.; Toncheva, A.; Dubois, P.; Raquez, J.-M. Shape-Memory Polymers For Multiple Applications In The Materials World. *Eur. Polym. J.* **2016**, *80*, 268−294.

(14) Nguyen, B. H.; Nguyen, V. H.; Tran, H. N. Rich Variety Of Substrates For Surface Enhanced Raman Spectroscopy. *Adv. Nat. Sci.: Nanosci. Nanotechnol.* **2016**, *7*, 033001.

(15) Li, J.-F.; Li, Z.-Y. Manipulation Of Plasmonic Wavefront And Light−Matter Interaction In Metallic Nanostructures: A Brief Review. *Chin. Phys. B* **2014**, *23*, 047305.

(16) Encina, E. R.; Coronado, E. A. Plasmon Coupling In Silver Nanosphere Pairs. *J. Phys. Chem. C* **2010**, *114*, 3918−3923.

(17) Li, G.; Zhu, R.; Yang, Y. Polymer Solar Cells. *Nat. Photonics* **2012**, *6*, 153−161.

(18) Liu, H.; Wang, D.; Song, Z.; Shang, S. Preparation Of Silver Nanoparticles On Cellulose Nanocrystals And The Application In Electrochemical Detection Of Dna Hybridization. *Cellulose* **2011**, *18*, 67−74.

(19) Habibi, Y.; Lucia, L. A.; Rojas, O. J. Cellulose Nanocrystals: Chemistry, Self-Assembly, and Applications. *Chem. Rev.* **2010**, *110*, 3479−3500.

(20) Querejeta-Fernández, A.; Chauve, G.; Methot, M.; Bouchard, J.; Kumacheva, E. Chiral Plasmonic Films Formed by Gold Nanorods and Cellulose Nanocrystals. *J. Am. Chem. Soc.* **2014**, *136*, 4788−4793.

(21) Wang, L.; Wang, W.; Di, S.; Yang, X.; Chen, H.; Gong, T.; Zhou, S. Silver-Coordination Polymer Network Combining Antibacterial Action And Shape Memory Capabilities. *RSC Adv.* **2014**, *4*, 32276−32282.

(22) Yu, Z.; Zhang, Q.; Li, L.; Chen, Q.; Niu, X.; Liu, J.; Pei, Q. Highly Flexible Silver Nanowire Electrodes for Shape-Memory Polymer Light-Emitting Diodes. *Adv. Mater.* **2011**, *23*, 664−668.

(23) Yu, Z.; Li, L.; Zhang, Q.; Hu, W.; Pei, Q. Silver Nanowire-Polymer Composite Electrodes for Efficient Polymer Solar Cells. *Adv. Mater.* **2011**, *23*, 4453−4457.

(24) Luo, H.; Li, Z.; Yi, G.; Wang, Y.; Zu, X.; Wang, H.; Huang, H.; Liang, Z. Temperature Sensing Of Conductive Shape Memory Polymer Composites. *Mater. Lett.* **2015**, *140*, 71−74.

(25) Luo, H.; Li, Z.; Yi, G.; Zu, X.; Wang, H.; Wang, Y.; Huang, H.; Hu, J.; Liang, Z.; Zhong, B. Electro-Responsive Silver Nanowire-

Shape Memory Polymer Composites. *Mater. Lett.* **2014**, *134*, 172−175.
(26) Lu, H.; Zhu, S.; Yang, Y.; Huang, W. M.; Leng, J.; Du, S. Surface Grafting Of Carbon Fibers With Artificial Silver-Nanoparticle-Decorated Graphene Oxide For High-Speed Electrical Actuation Of Shape-Memory Polymers. *J. Appl. Polym. Sci.* **2015**, *132*, 41673.
(27) Lu, H.; Liang, F.; Gou, J.; Leng, J.; Du, S. Synergistic Effect Of Ag Nanoparticle-Decorated Graphene Oxide And Carbon Fiber On Electrical Actuation Of Polymeric Shape Memory Nanocomposites. *Smart Mater. Struct.* **2014**, *23*, 085034.
(28) Zhang, H.; Zhao, Y. Polymers with Dual Light-Triggered Functions of Shape Memory and Healing Using Gold Nanoparticles. *ACS Appl. Mater. Interfaces* **2013**, *5*, 13069−13075.
(29) Zhang, H.; Zhang, J.; Tong, X.; Ma, D.; Zhao, Y. Light Polarization-Controlled Shape-Memory Polymer/Gold Nanorod Composite. *Macromol. Rapid Commun.* **2013**, *34*, 1575−1579.
(30) Xie, H.; Shao, J.; Ma, Y.; Wang, J.; Huang, H.; Yang, N.; Wang, H.; Ruan, C.; Luo, Y.; Wang, Q.-Q.; Chu, P. K.; Yu, X.-F. Biodegradable Near-Infrared-Photoresponsive Shape Memory Implants Based On Black Phosphorus Nanofillers. *Biomaterials* **2018**, *164*, 11−21.
(31) Yi, D. H.; Yoo, H. J.; Mahapatra, S. S.; Kim, Y. A.; Cho, J. W. The Synergistic Effect Of The Combined Thin Multi-Walled Carbon Nanotubes And Reduced Graphene Oxides On Photothermally Actuated Shape Memory Polyurethane Composites. *J. Colloid Interface Sci.* **2014**, *432*, 128−134.
(32) Cheng, Z.; Wang, T.; Li, X.; Zhang, Y.; Yu, H. NIR−Vis−UV Light-Responsive Actuator Films of Polymer-Dispersed Liquid Crystal/Graphene Oxide Nanocomposites. *ACS Appl. Mater. Interfaces* **2015**, *7*, 27494−27501.
(33) Lizundia, E.; Meaurio, E.; Vilas, J. L. Grafting of Cellulose Nanocrystals. In *Multifunctional Polymeric Nanocomposites Based on Cellulosic Reinforcements*; Puglia, D., Fortunati, E., Kenny, J. M., Eds.; William Andrew Publishing: Norwich, NY, 2016; Chapter 3, pp 61−113.
(34) Lokanathan, A. R.; Uddin, K. M. A.; Rojas, O. J.; Laine, J. Cellulose Nanocrystal-Mediated Synthesis of Silver Nanoparticles: Role of Sulfate Groups in Nucleation Phenomena. *Biomacromolecules* **2014**, *15*, 373−379.
(35) Noguez, C. Surface Plasmons on Metal Nanoparticles: The Influence of Shape and Physical Environment. *J. Phys. Chem. C* **2007**, *111*, 3806−3819.
(36) Ren, J.; Tilley, R. D. Preparation, Self-Assembly, and Mechanistic Study of Highly Monodispersed Nanocubes. *J. Am. Chem. Soc.* **2007**, *129*, 3287−3291.
(37) Abdallah, T.; El-Brolosy, T. A.; Mohamed, M. B.; Easawi, K.; Negm, S.; Talaat, H. Effect Of Shape And Interstice On Surface Enhanced Raman Scattering (Sers) Of Molecules Adsorbed On Gold Nanoparticles In The Near-Dipole And Quadrupole Regions. *J. Raman Spectrosc.* **2012**, *43*, 1924−1930.
(38) Lazko, J.; Sénéchal, T.; Landercy, N.; Dangreau, L.; Raquez, J.-M.; Dubois, P. Well Defined Thermostable Cellulose Nanocrystals Via Two-Step Ionic Liquid Swelling-Hydrolysis Extraction. *Cellulose* **2014**, *21*, 4195−4207.
(39) Vericat, C.; Vela, M. E.; Benitez, G.; Carro, P.; Salvarezza, R. C. Self-Assembled Monolayers Of Thiols And Dithiols On Gold: New Challenges For A Well-Known System. *Chem. Soc. Rev.* **2010**, *39*, 1805−1834.
(40) Dufresne, A. Cellulose Nanomaterial Reinforced Polymer Nanocomposites. *Curr. Opin. Colloid Interface Sci.* **2017**, *29*, 1−8.
(41) Lu, H.; Yao, Y.; Huang, W. M.; Leng, J.; Hui, D. Significantly Improving Infrared Light-Induced Shape Recovery Behavior Of Shape Memory Polymeric Nanocomposite Via A Synergistic Effect Of Carbon Nanotube And Boron Nitride. *Composites, Part B* **2014**, *62*, 256−261.
(42) Zhang, H.; Xia, H.; Zhao, Y. Optically triggered and spatially controllable shape-memory polymer-gold nanoparticle composite materials. *J. Mater. Chem.* **2012**, *22*, 845−849.
(43) Zhang, H.; Xia, H.; Zhao, Y. Light-Controlled Complex Deformation and Motion of Shape-Memory Polymers Using a Temperature Gradient. *ACS Macro Lett.* **2014**, *3*, 940−943.
(44) Weissleder, R. A. Clearer Vision For In Vivo Imaging. *Nat. Biotechnol.* **2001**, *19*, 316−317.
(45) Lendlein, A.; Langer, R. Biodegradable, Elastic Shape-Memory Polymers for Potential Biomedical Applications. *Science* **2002**, *296*, 1673−1676.
(46) Durán, N.; Durán, M.; de Jesus, M. B.; Seabra, A. B.; Fávaro, W. J.; Nakazato, G. Silver nanoparticles: A New View On Mechanistic Aspects On Antimicrobial Activity. *Nanomedicine* **2016**, *12*, 789−799.
(47) Willocq, B.; Bose, R. K.; Khelifa, F.; Garcia, S. J.; Dubois, P.; Raquez, J. M. Healing By The Joule Effect Of Electrically Conductive Poly(Ester-Urethane)/Carbon Nanotube Nanocomposites. *J. Mater. Chem. A* **2016**, *4*, 4089−4097.

DOI: 10.1021/acsami.8b10159
ACS Appl. Mater. Interfaces 2018, 10, 29933−29942